Journal of Solid State Electrochemistry
https://doi.org/10.1007/s10008-018-4050-8

ORIGINAL PAPER

Physical properties of silicene electrodes for Li-, Na-, Mg-, and K-ion batteries

Alexander Y. Galashev[1] · Alexey S. Vorob'ev[1]

Received: 26 January 2018 / Revised: 2 July 2018 / Accepted: 13 July 2018

Abstract
The transition from lithium-ion batteries to sodium- and potassium-ion batteries will increase the power of electrochemical current sources and the rate of their charging. On the basis of the first principles of density functional theory and ab initio molecular dynamics simulations, the interaction of Li, Na, Mg, and K atoms with an autonomous silicene has been studied. The adsorption energies and the Si–Me (Me = Li, Na, Mg, K) bond lengths for different locations of the adsorbed metal atoms are calculated. The favorable adsorption site of Me on silicene nanosheet is identified and reported. In the approximation of the generalized gradient, the band structure of the "silicene/Me" systems is calculated. The metallic state of an autonomous metallized silicene can arise for various cases of adsorption of an alkali metal and when the ratio between the Mg and Si atoms in the system is 1:1. Metallization of the semiconductor does not occur when the number of adsorbed Mg atoms is less than the number of Si atoms.

Keywords Density functional theory · Lithium · Potassium · Silicene · Sodium · Magnesium

Introduction

Demand for lithium-ion batteries (LIBs) is growing rapidly. Lithium-ion power sources are used in various electronic devices, including those for vehicles. However, lithium raw materials are limited and expensive. This problem is of particular interest for stationary applications, a basic requirement of which is low price. In this case, alternative energy-saving devices that use widely distributed elements are needed. Among these elements, alkali metals Na and K as well as Mg are suitable. The content of sodium, potassium, and magnesium in the Earth's crust is 2.3, 1.5 and 1.9%, respectively, while the content of lithium is only 0.00017%.

The creation of a cathode material for sodium-ion batteries (SIBs) is based on the use of metal oxides and polyanionic compounds [1, 2]. These materials have provided encouraging capacity and cyclic life. Currently, the anode part is the problematic part of SIBs. The maximum capacity of a Na/graphite cell used as the anode is only ~ 35 mA h / g, which is an order of magnitude lower than the capacity of the Li/graphite cell. In this instance, it is necessary to use expanded graphite, or use a solvent, the molecules of which are attached to graphite. Magnesium-ion batteries (MIBs) have several advantages over lithium-ion batteries. MIBs are more stable, due to the fact that the magnesium melting point is higher than that of lithium, but most importantly the energy density of magnesium-ion battery can be five times higher than today's lithium-ion ones [3]. Magnesium metal does not form dendrites and, in addition, has higher volumetric energy density than lithium metal. Much more abundance of magnesium than lithium leads to reduction of raw material costs. In the process of creating potassium-ion batteries (PIBs), the experience of unsuccessful use of graphite in SIBs is taken into account. The possibility of the intercalation of potassium into graphite is immersed in KF or KF/AlF_3 melts at temperatures above 700 °C. However, at room temperature, it is necessary to use a non-graphite material, for example, carbon fibers (soft graphite) [4].

In work [5], it was proposed to use an asymmetric intercalation battery with $K_2NiFe(CN)_6$ as the cathode, commercial graphite as an anode, and an organic electrolyte comprising a

✉ Alexander Y. Galashev
galashev@ihte.uran.ru

[1] Institute of High-Temperature Electrochemistry, Ural Branch, Russian Academy of Sciences, Sofia Kovalevskaya Str. 22, Yekaterinburg, Russia 620990

Published online: 21 July 2018

mixed salt of lithium and potassium. The battery operates by two reversible simultaneous intercalations. There are K^+ ions at the cathode and Li^+ ions at the anode. The coordination medium of π-electrons in $K_2NiFe(CN)_6$ provides the preferred reversible intercalation of K^+ ions, while the small ionic radius creates the preferred reversible intercalation of the Li^+ ion in graphite. The battery shows a high operating voltage (~ 3.6 V) and a long service life with a minimal power decreases even after 5000 cycles.

Graphite anodes have a relatively low capacity due to the limited number of ion storage sites within the hexagonal carbon structure [6]. The current capacity of the anode battery can be theoretically increased by replacing the carbon anode material by a new silicene [7–9] one. Silicene is the silicon counterpart of graphene, i.e., of consists in a single layer of Si atoms with a hexagonal arrangement. Silicene has attracted extensive interest due its massless Dirac Fermion characteristics [10], strong spin–orbital coupling (SOC) [11], and great potential in electronic applications [12].

The early successful production of silicene disproves the generally accepted view of hybridization—substantiation that silicon atoms can form a hybridized sp^2–sp^3 state and crystallize into a two-dimensional structure [13, 14]. The first part of the process of intercalation of alkali metal ions in a silicon material is the reduction of these ions to atoms at the boundary between the anode and the electrolyte. The second one is the diffusion of the alkali metal into the anode material.

The aim of this work is to research the interaction of Li, Na, K, and Mg atoms with freestanding (without substrate) silicene, in order to determine the adsorption and electronic properties of silicene. This will be important part of an investigation of Si-based anodes.

Computer model

Our calculations were performed using the SIESTA [15, 16] package, which implements density functional theory (DFT) with the pseudopotential approximation and a basis set of linear combination of atomic orbital [17, 18]. The calculations with a nonlocal potential were carried out within the framework of the generalized gradient approximation (GGA) [19]. To improve the computational speed, we performed geometric optimization using the Purdue–Burke–Erzerhof procedure (PBE) [20]. The tolerances for optimizing the geometry at full energy were within 5.0×10^{-6} eV/atom. The maximum Hellmann–Feynman force was within 0.01 eV · $Å^{-1}$, the maximum displacement of the atom did not exceed 5.0×10^{-4} Å, and the maximum stress was within 0.02 GPa. The geometry of all structures was completely optimized. To calculate all the properties, a single silicene cell consisting of eight atoms and periodic boundary conditions (PBC) was used. The initial coordinates of the four Si atoms of the unit cell were shifted to a distance of 0.064 nm perpendicular to the surface, and the remaining Si atoms were on the same (initial) plane. Such a structure of the silicene sheet is close to the surface of the silicene observed on the Ag (111) substrate [21]. In other words, the reconstruction of the surface $\sqrt{3} \times \sqrt{3}$ [22] was considered. After geometry optimization, the obtained adsorption sites were tested for thermal stability by constant-temperature molecular dynamics, known as Nose–Hover thermostat [23]. The temperature of thermostat was chosen as 293 K. The duration of the calculation was 2000 time steps. The time step length was 1 fs.

The energy of adsorption of Me (lithium, sodium, magnesium, and potassium) atoms on the silicon surface was calculated according to the following expression:

$$E_{ad} = (E_{Si} + nE_{Me} - E_{Si+Me})/n$$

where E_{Si+Me} and E_{Si} are the total energies of the silicon surface with and without Me ad-atoms, respectively, E_{Me} is the energy of alkali metal atoms calculated with spin polarization, and n is the number of adsorbed Me atoms.

In the inverse spatial expansion of the charge density, a cutoff on the grid equal to 2720 eV was used. The Brillouin zone (BZ) was introduced using a matrix of $10 \times 10 \times 1$ k-points in the Monocharst–Pack module. To carry out all calculations, the method of diagonalization was applied. The band structure was obtained in the direction of the *K*–*Γ*–*M*–*K* of the singular points of the BZ in all the systems examined.

The density of states (DOS) of a system describes the number of states per interval of energy at each energy level available to be occupied. A density distribution is an average over the space and time domains of the various states occupied by the system. A high DOS at a specific energy level means that there are many states available for occupation. A DOS of zero means that no states can be occupied at that energy level. Charge carriers move between valence band (VB) and conduction band (CB) under thermal influence. In the dark and at equilibrium, the concentration of electrons and holes is unaffected by these processes. Generation, under influence of light absorption for example, promotes electrons from the valence band to the conduction band, resulting in a new free electron in the CB, and a new hole in the VB. There is a certain difference between the calculated density of states of a substance and its photoemission spectrum (PES). PES consists of two principal components: (i) primary electrons which did not suffer inelastic collisions, and (ii) secondary electrons (primary electrons, which lost varying amounts of energy). The primary electrons result in distinct spectral features (peaks) mirroring (in first order approximation) DOS of the sample, while secondary electrons have a more or less continuous energy spectra down to zero kinetic energy, which is superimposed to the primary electron spectrum.

Understanding of the band structure of the new nanomaterials is essential to have a deeper insight into their optical and electrical properties. As a rule, the systems considered by us do not have a direct band gap (BG). Therefore, we determine the width of the BG as $E_g = \min(E_c - E_v)$, where E_c and E_v are the current values of the energy of the conduction and valence bands, respectively. The values of E_c and E_v energies are considered in the *K*–*Γ*–*M*–*K* direction. We assume that at the Fermi level the total number of electrons in the conduction band is equal to the total number of holes in the valence band. It should be noted that, although DFT underestimates the energy gap E_g, the method used by us can give exact values of E_g for many semiconductors [24, 25]. In addition, it was used to describe the electronic properties of materials based on graphene, with accuracy comparable to GW (a combination of the Green's function *G* and the screened Coulomb interaction W) [26]. To confirm the reliability of this method, we performed calculations for bulk Si as a standard, because of the lack of experimental data for silicene. For bulk silicon, $E_g = 1.034$ eV, which is close to the experimental result of 1.17 eV [27].

One of the classifications of semiconductors is on the basis band gaps. The minimum energy gap is the difference in energy between the conduction band edge and the valence band edge. If both the band edges are at the same *k*-point of the Brillouin zone, the band gap is direct. If these differ by a finite wave vector, the band gap is indirect. These can be determined by optical absorption experiments. If one plots the coefficient of optical absorption as a function of photon frequency and notices a sudden steep rise in absorption, the frequency corresponds to direct band gap energy. If, however, at first there is a small gradual rise in a frequency range followed by a sudden rise, the spectrum corresponds to an indirect band gap. The frequency at which the absorption coefficient starts rising gradually is the measure of the indirect gap. In indirect band gap semiconductor, in addition to a photon, a phonon is also involved in the conservation rules for the momentum and energy.

There are many possible sites for a metal atom to occupy. Five non-equivalent adsorption sites (Fig. 1) are investigated: I and II—the metal ad-atom is located above the silicon atom of the upper and lower sublattices, respectively; III—the metal ad-atom is above the geometric center of the six-link ring; IV—the ad-atom of the metal is above the midpoint between two neighboring atoms; V—atom of a metal replaces one of the silicon atoms; VI—doping of silicene with metal atoms in the ratio 1 Me:2 Si (all Me atoms were located in positions II); and VII—system with the ratio of atoms 1 Me:1 Si. The use of PBC leads to the fact that the number of ad-atoms in the model for cases I–IV is one-quarter of all Si atoms, and for the case V, the number of substituting atoms is one-third of Si atoms.

The number of absorption sites for metal atoms can be increased by depositing metal atoms on the back of the

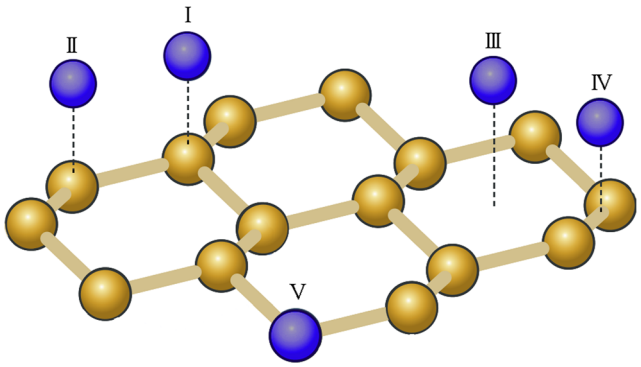

Fig. 1 Preferable adsorption sites are as follows: I and II—the metal ad-atom is located above the silicon atom of the upper and lower sublattices, respectively; III—the metal ad-atom is above the geometric center of the six-link ring; IV—the ad-atom of the metal is above the midpoint between two neighboring atoms; and V—the atom of a metal replaces one of the silicon atoms

silicene sheet. Getting the largest population of metal atoms is important to achieve the maximum charge capacity of the battery. Therefore, in the present study, we consider the number of sites suitable for the adsorption of metal atoms, which is twice the number of Si atoms in silicene. To study the charge capacity of metal-ion batteries, the Hirshfeld atomic population analysis [28] was done for additional silicene-metal systems. The Hirshfeld population analysis scheme carves the molecular density into atomic density contributions. This method does not require a reference to basis sets or their respective locations, but is based on a different physical and mathematical footing. The advantage of this method is that, when the molecular deformation density converges to the true solution, the computed net charges will necessarily converge. This method also allows a straightforward definition for "local" moments. The charges found in the Hirshfeld method are smaller than those from the other methods, for example, in the conventional Mulliken and Löwdin population analyses.

The ratio of metal atoms to silicon atoms in these systems varied from 1:8 to 18:8. We used the following systems: (i) first one with atomic ratio 1:8 containing ad-atom of metal above the geometric center of the six-link silicon ring, (ii) systems with the ratio from 2:8 to 9:8 that in addition to the ad-atom located above the center of the ring have the metal ad-atoms in front of nodes of the lower silicene sub-lattice on both sides of the autonomous silicene sheet, (iii) for systems having the atomic ratio from 10:8 to 17:8, we similarly added metal atoms to the position in front of the nodes of the higher silicene sub-lattice, and (iv) finally, the position below the geometric center of the six-link silicon ring were chosen for one more addition in the case of the system with ratio of metal-silicon atoms of 18:8. All systems were geometrically optimized.

The calculations were performed on a hybrid cluster-type computer "URAN" at the IMM UB RAS with a peak performance of 216 Tflop / s and 1864 CPUs.

Results and discussion

As we move down the group (Li, Na, K, Rb, Cs), the ionization energy decreases and, consequently, the reactivity of metals increases. So the energies of the first ionization of Li, Na, Mg, and K are equal to 5.41, 5.16, 4.61, and 4.36 eV, respectively. During the reaction, these metals form positive ions and the lower the ionization energy, the easier the formation of these ions. However, the formation of a positive ion is only one stage of a multistage process. Therefore, the choice of a reaction type can be made by considering the whole picture, and not one of its small parts. Nevertheless, the ionization energies of the elements are the main factors affecting the activation energy of the reaction, i.e., minimum energy required to initiate a reaction. The lower the activation energy, the faster the reaction will occur.

The layer of atoms formed on the surface during physical adsorption is bound to the surface by weak interatomic bonds, which are to a small degree capable of balancing uncompensated bonds of surface atoms. The process of physical adsorption is an isothermal, inactive process. Moreover, the "gas" on the given crystalline surface is adsorbed. The easier, the higher its boiling point is, i.e., the easier it turns into a liquid. The boiling point decreases in the Li, Mg, Na, K series in accordance with the values 1370, 1090, 890, and 770 (°C). Among the metals considered, lithium is the most readily adsorbed, and potassium is the most difficult to adsorb. Adsorption reduces surface energy. At the same time, some amount of energy is released into the environment, called the adsorption energy. Energy (heat) of physical adsorption, as a rule, is small and rarely exceeds several tenths of eV (about 0.4 eV).

The calculated adsorption energies of Li, Na, Mg, and K atoms for silicene are shown in Fig. 2. The adsorption (activation) energy of alkali metals (Li, Na, and K) decreases with increasing atomic number of the element. It can be seen that with insufficiently intense adsorption of the Hollow type, which, in particular, is most likely to occur at the initial stage of filling the surface of a silicene electrode with metal, magnesium has a noticeable advantage over alkali metals. Depending on the place of adsorption, the adsorption energy of magnesium is closer to that of lithium, sodium, or potassium. The checking for thermal stability of the seven selected adsorption sites showed that only four cases (III, V, VI, VII) are possible, whereas the configurations for the cases I, II, and IV during the MD calculation are transformed to the case III configuration. The position above the center of the hexagonal ring (the III case) is the only possible site for the Li, Na, and Mg ad-atoms in the case of initial adsorption in the form of I, II, IV, or V. Adsorption energy for this position for Li and Na equals to 2.082 eV and 1.65 eV respectively, which is sufficiently close to the results (2.08 and 1.58 eV) obtained in [29, 30]. At the same time, the ab initio MD simulation showed that the potassium atom can be adsorbed in both III and V positions.

Due to the considerable difference in the sizes of the atoms of the metals studied, the lengths $L_{Si–Me}$ of the Si–Me bonds for the considered options of the arrangement of the Me atoms have a regularity (Fig. 3). As can be seen from the figure, for all the options considered, a strict relationship is observed: $L_{Si–K} > L_{Si–Na} > L_{Si–Li}$, while the length of the Si–Mg bond, as well as the adsorption energy, do not have a clear pattern. For the Na and K atoms the lowest $L_{Si–Me}$ is observed in the "Hollow" position (III) while for the Li and Mg ones are observed in the "Full" and "Half" position (VII and VI), respectively. The greatest value of $L_{Si–Me}$ was obtained when Li or Na atoms were deposited on silicene in a ratio of two silicene atoms to one Li (Na) atom. However, in the case of adsorption of K atoms, the greatest value of $L_{Si–K}$ is detected

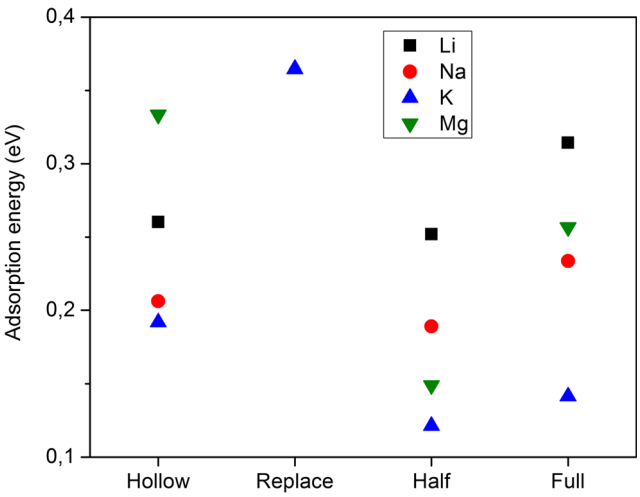

Fig. 2 The adsorption energy of Li, Na, Mg, and K atoms optimized using the GGA method and ab initio MD, depending on the location of these atoms relative to the silicene supercell

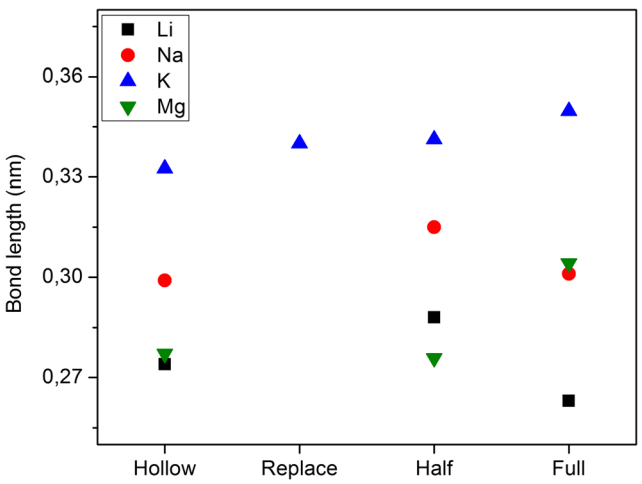

Fig. 3 The length of the Si–Me bond for Li, Na, Mg, and K atoms optimized using the GGA method and ab initio MD, depending on the location of these atoms relative to the silicene super cell

when adsorption to silicene occurs in the ratio of one atom K to one Si atom. At the same time, $L_{Si–Mg}$ is significantly larger than $L_{Si–Li}$ only in the case of adsorption going according to option VII. The greater remoteness of Na and, especially, K atoms from silicene promotes their faster adsorption and also desorption than that is the case for Li atoms. This also contributes to an increase in the effective charge transfer rate in the electrochemical source of current, and hence, to the increase in the battery power.

To date, the most of the research devoted to the search for new materials for the anode of ionic batteries has been performed for electrochemical devices in which charge carriers are lithium ions. With traditional graphite anodes, lithium ions accumulate around the outer surface of the anode. Silicene has a more elegant solution by enabling lithium ions to pass through the tiny holes of the silicene sheets measuring 10–20 nm. This promises optimal storage area and easy extraction. Once available, such a battery is estimated to store more than ten times more energy than Li-ion featuring regular graphite anodes. Although the electronic conductivity of the anode material does not have a significant effect on the rate of charging/discharging of ionic batteries, it can affect secondary processes, leading to a decrease in the number of charge carriers and, consequently, to a loss of electrical capacitance. Therefore, information on the electronic conductivity of the anode, including when it is filled with charge carriers (ions), is important for the choice of the anode material and the composition of the electrolyte. Crucial to the conduction process is whether or not there are electrons in the conduction band. In insulators, the electrons in the valence band are separated by a large gap from the conduction band, in conductors like metals the valence band overlaps the conduction band, and in semiconductors there is a small enough gap between the valence and conduction bands that thermal or other excitations can bridge the gap. With such a small gap, the presence of a small percentage of a doping material can increase conductivity dramatically.

The freestanding (autonomous) silicene has the band gap width of a zero or close to it and a linear dispersion at the point *K* [31, 32]. Since the effective spin–orbit interaction is quite significant in silicene compared to graphene, buckling in silicene opens a gap of 1.55 meV at the Dirac point. This band gap can be further tailored by applying in plane stress, an external electric field, and chemical functionalization and defects. Lithium adsorption by silicene can significantly change its electronic properties up to the transition from the metallic state to the narrow-band semiconductor with an increase in the number of Li atoms to reach a concentration satisfying the ratio 1 Li:1 Si (Fig. 6a). This is due to the complete compensation of unsaturated bonds in silicene by lithium. Calculations show that silicene with adsorbed Na or K in the cases considered by us should exhibit the properties of a conductor (Figs. 4, 5, 6, 7). While Mg atom adsorption only in one of the cases creates to conductor properties (Fig. 6) and conductor properties (Fig. 6), in the other two options the adsorption of magnesium on silicene leads to an increase of width of the band gap (Figs. 4, 5). In cases III, VI magnesium systems have indirect band gaps equal to 0.767 eV and 0.547 eV, respectively. On the other hand, Li systems have conductor properties in cases III and VI (Figs. 4, 5) and semiconductor ones in case VII with width of the direct band gap equal to 0.388 eV (Fig. 6).

The adsorption energy for metal atoms on silicene with the different ratio of the number of metal ad-atoms to silicon atoms is shown in Fig. 8. As can be seen from Fig. 8, at the ratio of 1 Me:8 Si atoms, the adsorption energy of each of the metals under consideration is lower than at the ratio of 2 Me:8 Si. However, a further increase in the number of adsorbed atoms Me usually leads, not to an increase in the specific adsorption energy, but to its decrease. When Mg, Na, and Li are adsorbed, the decrease in E_{ad} ceases at $N_{Me}/N_{Si} = 11/8$, 13/8, and 15/8, respectively. In the case of adsorption of K, however, the energy E_{ad} as a whole continues to decrease until $N_{Me}/N_{Si} = 18/8$. Moreover, a decrease in the energy E_{ad} with an increase in N_{Me}/N_{Si} during adsorption of K occurs faster than a decrease in the energy upon adsorption of other metals. This is mainly due to the large size of the K atom compared to the size of the atoms of other metals in question. Because of the large size, the deposited atoms of K are removed from the surface of the silicene farther than the atoms of the other metals. Their interaction with the surface is also weaker. In this case, the dependence on the number of adsorbed atoms becomes stronger. An energetic regularity is retained for the alkali metals—an element with a large atomic number has a lower adsorption energy for any ratio of N_{Me} to N_{Si}.

Figure 9 shows the specific charge transfer from metal ions to silicon atoms, depending on the number of metal ions adsorbed on the surface of the silicene. From the results presented in the Fig. 9, it can be seen from the Fig. 9 that the specific charge carried by a single adsorbed metal ion in all the cases considered is less than the corresponding value observed when two ions are adsorbed. However, with a further increase in the number of adsorbed ions from 2 to 14, the transferred specific charge of an alkali metal is reduced, and when the number of precipitating ions is greater than 14, the specific charge does not change much. Besides, the value of the specific charge for Li^+, Na^+, and K^+ is close when 18 ions are adsorbed. For the Mg^{2+} ions, this value is almost doubled. We notice that there is regularity in the distribution of the specific charge of alkali metal ions—the more massive the ion, the less charge it transfers to silicon atoms. The charge/N_{Me}(N_{Me}) function for Mg^{2+} has a steeper descending behavior for $N_{Me} < 9$ and slightly changes for $N_{Me} > 11$. The local maximum of this function appears for $N_{Me} = 10$.

Silicene possesses predicted electron transport properties similar to graphene, as well as the advantage of compatibility

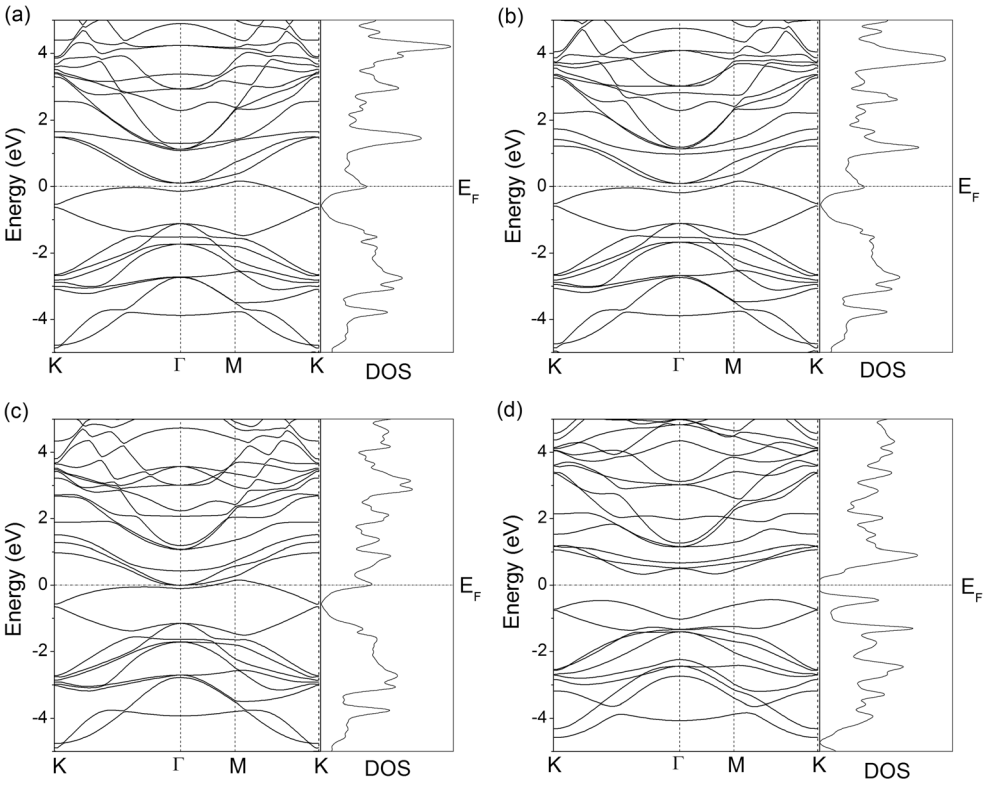

Fig. 4 Density of states (DOS) and energy bond structure of silicene with the ad-atom of metal (Li, Na, Mg and K) located above the geometric center of the six-link ring, obtained with the help of GGA, where **a** –Li, **b** – Na, **c** – K, **d** – Mg. The Fermi energy is set to zero

with existing silicon-based technology. The change in the band structure of silicene, when sodium is adsorbed in the ratio 1 Na:1 Si does not fundamentally change the already high electrical conductivity of this material. This also does not affect its ability to be used as the anode material of the SIB. Additionally, the inversion symmetry breaking imparted

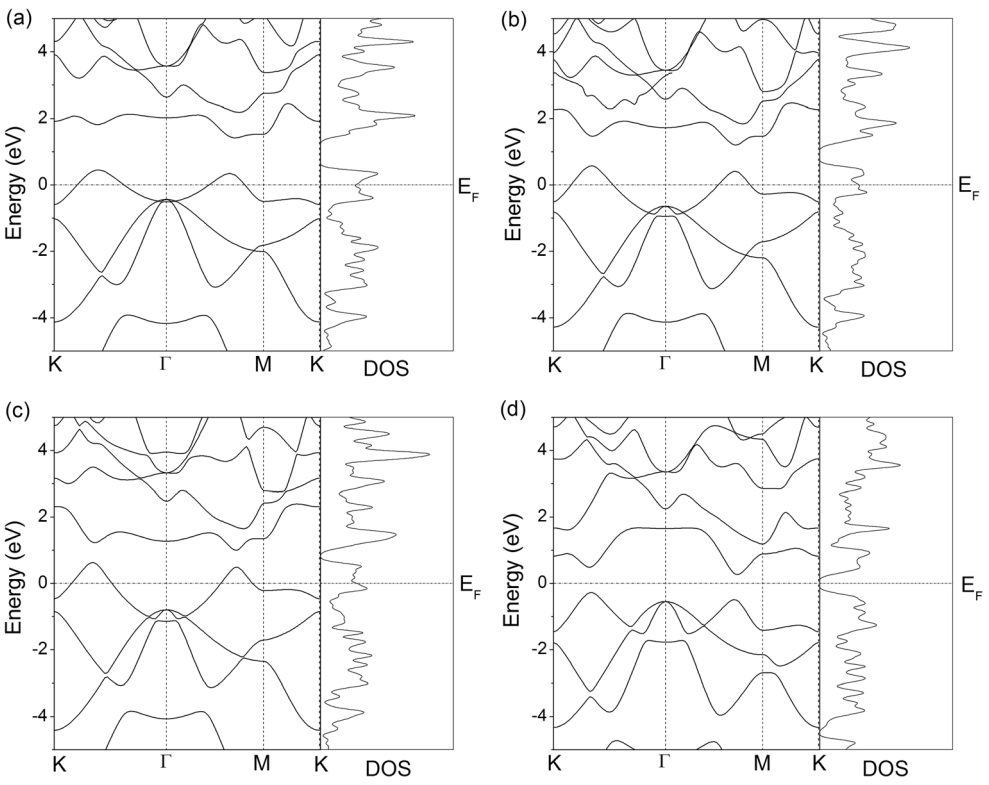

Fig. 5 Density of states (DOS) and energy bond structure of the "silicene/Me" system with the ratio of atoms 1 Me:2 Si, obtained with the help of GGA, where **a**, Li; **b**, Na; **c**, K, and **d**, Mg. The Fermi energy is set to zero

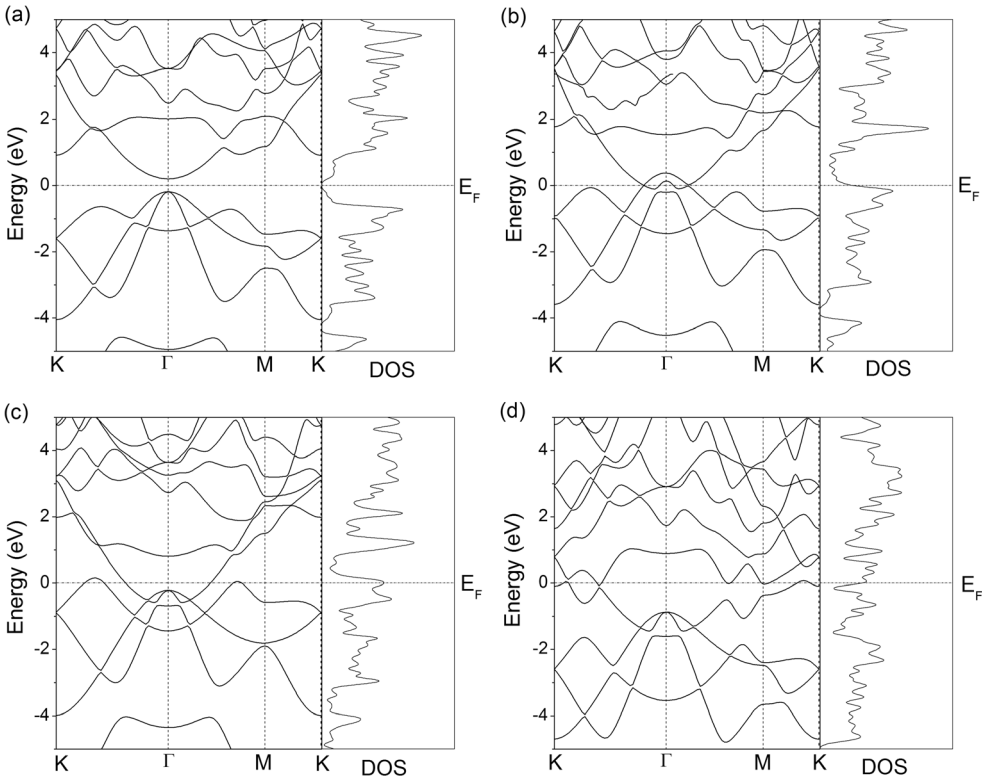

Fig. 6 Density of states (DOS) and energy bond structure of the "silicene/Me" system with the ratio of atoms 1 Me:1 Si, obtained with the help of GGA, where **a**, Li; **b**, Na; **c**, K, and **d**, Mg. The Fermi energy is set to zero

by the buckled lattice structure may be taken advantage of through the application of an external electrical field perpendicular to the plane for fine control for the width of the band gap [33].

There is a ratio of 1:0.54:0.29 between the concentrations of free electrons in Li, Na, K metals, and for Fermi energies it is of 1:0.65:0.44 and for relative electronegativities it is 1:0.9:0.8. The difference of these properties between the Li, Na, and K atoms, along with the difference in the atomic dimensions, leads to their differentiated effects on the band structure when adsorbing alkali metal atoms on silicene. It is known that the surfaces of semiconductors are the subject to reconstruction, which can be dramatically altered by the presence of the adsorbed metal atoms [34]. With appropriate doping, the Fermi level can be shifted to the BG, as a result of which, in some cases, the state of the degenerate gas in the conduction band or in the valence band is reached. In semiconductors, especially with a wide BG, the Fermi energy can be easily shifted by several eV. The Fermi level can be free or fixed

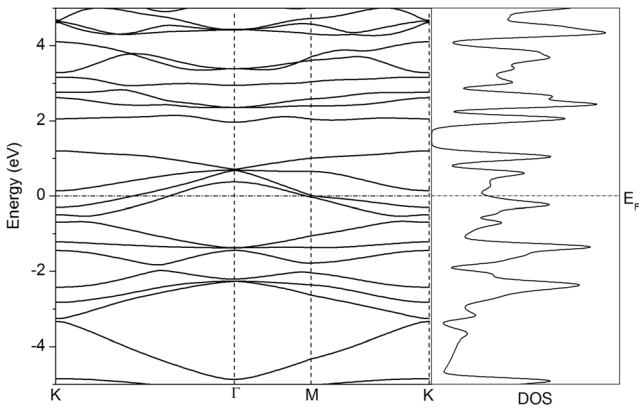

Fig. 7 Energy bond structure and density of states obtained with the help of GGA for the silicene when 1 Si atom is replaced by a K atom

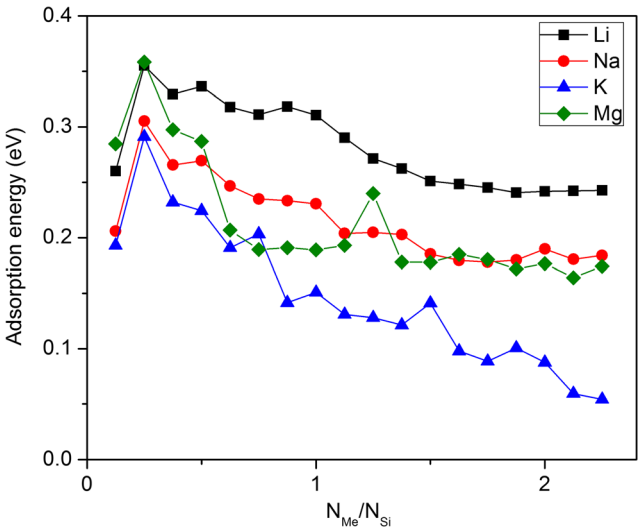

Fig. 8 Adsorption energy of Me (Li, Na, Mg, K) atoms, where N_{Me} is quantity of metallic atoms, N_{Si} is quantity of silicon atoms (always equal to eight)

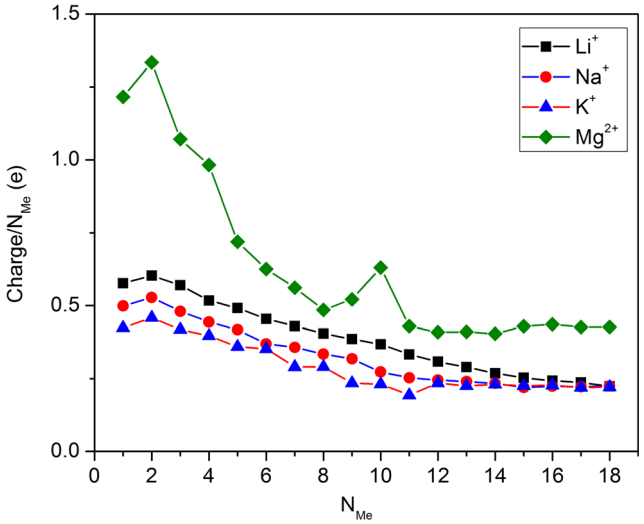

Fig. 9 The charge distributed from metallic ions to the silicon atoms is counted by Hirshfeld atomic population analysis divided by the number of metal atoms, where Me is Li^+, Na^+, Mg^{2+}, K^+, and N_{Me} is a quantity of metallic ions and "Charge" is the elementary charge distributed on silicon

surface states, which entails the transfer of charge to the surface or, conversely, from the surface. By properly manipulating ad-atoms by changing their location or charge, the average electric field inside the silicene can be changed [35, 36]. A special case of an explicit overlap of the valence band with the conduction band was observed as a result of the adsorption of Na atoms on silicene in a 1:1 ratio. A set of closely contiguous states is formed in this case, exceeding the number of electrons contained in them, i.e., the "silicene/Na" system acquires metallic properties. The position of the Fermi level is associated with the energy of adsorption of various atoms or ions. The change in the Fermi level due to the doping creates great difficulties in deciphering the band structure of the semiconductor.

The energy of adsorption of magnesium atoms on the silicene is close to that of sodium. However, the transfer of a charge from magnesium atoms to silicon atoms is much higher than this value for sodium or lithium, including in the region of abundant metal adsorption (~2 Me:1 Si), where carried charge doubles. This fact underscores the prospect of using magnesium-ion batteries. Typical Li-ion cathode materials are not compatible with Mg-ion due to its sluggish kinetics of insertion/desertion of magnesium ions in the cathode materials. In connection with this, to date, it has not been possible to achieve acceptable performance of the Mg-ion batteries.

Conclusions

Battery chemistry based on earth-abundant elements has great potential for the development of cost-effective, large-scale energy storage systems. Our investigation showed promising features that could give a new future to silicon in the electronics industry, thus opening a promising route toward wide-range applications including the use of silicene in the material of the anode of ionic batteries. Due to the natural abundance and low cost compared with lithium, the sodium-, magnesium-, and potassium-ion batteries show great potential to be used in grid storage, where a fast charge/discharge rate and long cycling life are required. Graphite has a very low capacity when used as a Na-ion battery anode. Electrochemical insertion of Na into graphite is significantly hindered by the insufficient interlayer spacing. Expanded graphite has an enlarged interlayer lattice distance and retains an analogous long-range-ordered layered structure. The Na-ion can be reversibly inserted into and extracted from expanded graphite. Na-ion batteries are promising candidates to replace Li-ion batteries in large-scale applications. The calculated Na capacity for freestanding silicene is highly competitive and exceeds the corresponding value of expanded graphite by factor 3.3. Soft graphite is able to store K^+ and deliver a relatively large capacity. PIB could be a better choice in terms of energy density. Exploring stable and reversible anodes beyond a conventional category is of great interest. However, there are significant difficulties due to the lack of a necessary candidate with high potassium storage capability and extraordinary stability, as well as the sluggish kinetics of K^+ intercalating into the electrode host material. Suitable electrode materials must have thermodynamic or kinetic priority for intercalation of a targeted cation as well as excellent cycling stability. The thermodynamic priority mainly depends on the reaction energy and chemical potential for cation storage in the electrode materials, which is correlated with the kind of redox couples for transition metals and the cation coordination environments. The kinetic priority is mainly determined by an ability of the cation diffusion, as well as efficiency of the reversible phase transition leading to the formation and destruction of intermediate phases. Our calculations show that silicene is a suitable material for the anode, not only LIB, but also SIB, MIB, and PIB. The next task is to choose the most suitable substrate for the use of silicene in electrochemical energy storage devices. First-principle modeling is a powerful tool for battery research as it can accurately study the structural and electronic properties of electrode and electrolyte materials as well as the interactions between different materials. It can be used for fast screening of materials with desired properties to speed up the search for useful materials to make Mg-ion batteries a reality sooner.

Funding information The study was performed by the grant from the Russian Science Foundation (Project No. 16-13-00061).

References

1. Xia X, Dahn JR (2012) NaCrO2 is a fundamentally safe positive electrode material for sodium-ion batteries with liquid electrolytes. Electrochem Solid-State Lett 15(1):A1–A4
2. Kim J, Seo D-H, Kim H, Park I, Yoo J-K, Jung S-K, Park Y-U, Coddard WA III, Kang K (2015) Unexpected discovery of low-cost maricite $NaFePO_4$ as a high-performance electrode for Na-ion batteries. Energy Environ Sci 8:540–545
3. Andrews JL, Mukherjee A, Yoo HD, Parija A, Marley PM, Fakra S, Prendergast D, Cabana J, Klie RF, Banerjee S (2018) Reversible Mg-ion insertion in a metastable one-dimensional polymorph of V_2O_5. Chem 4(3):564–585
4. Jian Z, Luo W, Ji X (2015) Carbon electrodes for K-ion batteries. J Am Chem Soc 137:11566–11569
5. Zheng J, Deng W, Hu Z, Zhuo Z, Liu F, Chen H, Lin Y, Yang W, Amine K, Li R, Lu J, Pan F (2018) Asymmetric K/Li-ion battery based on intercalation selectivity. ACS Energy Lett 3(1):65–71
6. Galashev AE, Zaikov Yu P (2015) Computer simulation of Li^+ ion interaction with a graphene sheet. Rus J Phys Chem A 89:2243–2247
7. Galashev AE, Zaikov Yu P, Vladykin RG (2016) Effect of electric field on lithium ion in silicene channel. Computer experiment. Russ J Electrochem 52(10):966–974
8. Galashev AE, Ivanichkina KA, Vorobiev AS, Rakhmanova OR (2017) Structure and stability of defective silicene on Ag(001) and Ag(111) substrates: a computer experiment. Phys Solid State 59(6):1242–1252
9. Galashev AE, Ivanichkina KA (2017) Computational study of the properties of silicon thin films on graphite. Rus J Phys Chem A 91(12):2448–2452
10. Chen L, Liu C-C, Feng BJ, He X, Cheng P, Ding ZJ, Meng S, Yao YG, Wu KH (2012) Evidence for Dirac fermions in a honeycomb lattice based on silicon. Phys Rev Lett 109:056804
11. Liu CC, Feng W, Yao YG (2011) Quantum spin hall effect in silicene and two-dimensional germanium. Phys Rev Lett 107: 076802
12. Tao L, Cinquanta E, Chiappe D, Grazianetti C, Fanciulli M, Dubey M, Molle A, Akinwande D (2015) Silicene field-effect transistors operating at room temperature. Nat Nanotechnol 10:227–231
13. Vogt P, De Padova P, Quaresima C, Avila J, Frantzeskakis E, Asensio MC, Resta A, Ealet B, Le Lay G (2012) Silicene: compelling experimental evidence for graphenelike two-dimensional silicon. Phys Rev Lett 108:155501
14. Meng L, Wang Y, Zhang L, Du S, Wu R, Li L, Zhang Y, Li G, Zhou H, Hofer WA, Gao H-J (2013) Buckled silicene formation on Ir(111). Nano Lett 13:685–690
15. Ordejon P, Artacho E, Soler JM (1996) Self-consistent order-N density-functional calculations for very large systems. Phys Rev B 53:10441–10444
16. Sanchez-Portal D, Ordejon P, Artacho E, Soler JM (1997) Density functional method for very large systems with LCAO basis sets. Int J Quantum Chem 65:453–461
17. Hohenberg P, Kohn W (1964) Inhomogeneous electron gas. Phys Rev B 136:864–871
18. Kohn W, Sham LJ (1965) Self-consistent equations including exchange and correlation effects. Phys Rev A 140:1133–1138
19. Filippi C, Singh DJ, Umrigar CJ (1994) All-electron local-density and generalized-gradient calculations of the structural properties of semiconductors. Phys Rev B 50:14947–14951
20. Perdew JP, Burke K, Ernzerhof M (1996) Generalized gradient approximation made simple. Phys Rev Lett 77:3865–3868
21. Kawahara K, Shirasawa T, Arafune R, Lin C-L, Takahashi T, Kawai M, Takegi N (2014) Determination of atomic positions in silicene on Ag(111) by low-energy electron diffraction. Surf Sci 623(3):25–28
22. Cahangirov S, Ozcelik VO, Xian L, Avila J, Cho S, Asensio MC, Ciraci S, Rubio A (2014) Atomic structure of the $\sqrt{3} \times \sqrt{3}$ phase of silicene on Ag(111). Phys Rev B 90:035448
23. Nose S (1984) A unified formulation of the constant temperature molecular dynamics methods. J Chem Phys 81:511–519
24. Asahi R, Mannstadt W, Freeman AJ (1999) Optical properties and electronic structures of semiconductors with screened-exchange LDA. Phys Rev B Condens Matter 59:7486–7492
25. Seidl A, Görling A, Vogl P, Majewski JA, Levy M (1996) Generalized Kohn–Sham schemes and the band-gap problem. Phys Rev B Condens Matter 53:3764–3774
26. Leng X, Jin F, Wei M, Ma Y (2016) GW method and Bethe–Salpeter equation for calculating electronic excitations. Comp Mol Sci 6(5):532–550
27. Yan JA, Yang L, Chou MY (2007) Size and orientation dependence in the electronic properties of silicon nanowires. Phys Rev B: Condens Mater 76:115319
28. Hirshfeld FL (1977) Bonded-atom fragments for describing molecular charge densities. Theor Chim Acta 44(2):129–138
29. Mortazavi B, Dianat A, Cuniberti G, Rabczuk T (2016) Application of silicene, germanene and stanene for Na or Li ion storage: a theoretical investigation. Electrochim Acta 213:865–870
30. Tritsaris GA, Kaxiras E, Meng S, Wang E (2013) Adsorption and diffusion of lithium on layered silicon for Li-ion storage. Nano Lett 13:2258–2263
31. Rowe JE (1974) Photoemission measurement of surface states for annealed silicon. Phys Lett A 46(6):400–402
32. Rowe JE, Ibach H (1974) Surface and bulk contributions to ultraviolet photoemission spectra of silicon. Phys Rev Lett 32(8):421–424
33. Tim HO, Farajian AA (2012) Stability of lithiated silicene from first principles. J Phys Chem C 116:22916–22920
34. Galashev AE, Rakhmanova OR, Zaikov Yu P (2016) Defect silicene and graphene as applied to the anode of lithium-ion batteries: numerical experiment. Phys Solid State 58(9):1850–1857
35. Galashev AY, Ivanichkina KA (2017) Nanoscale simulation of the lithium ion interaction with defective silicone. Phys Lett A 381: 3079–3083
36. Rakhmanova OR, Galashev AE (2017) Motion of a lithium ion over a graphene–silicene channel: a computer model. Rus J Phys Chem A 91(5):921–925